

Directional Design of Materials Based on the Pareto Optimization: Application to Two-Dimensional Thermoelectric SnSe

Shenshen Yan,* Zhibin Gao,* Yang Long, and Jie Ren†

Center for Phononics and Thermal Energy Science, China-EU Joint Center for Nanophononics,

Shanghai Key Laboratory of Special Artificial Microstructure Materials and Technology,

School of Physics Sciences and Engineering, Tongji University, Shanghai 200092, China

(Dated: December 14, 2024)

Increasing the efficiency of directional design of functional materials is a challenging work in theory, whose performance and stability are determined by different factors entangled with each other complicatedly. In this work, we apply the Pareto Optimization based on the Pareto Efficiency and Particle-Swarm Optimization to design new functional materials directionally. As a demonstration, we apply the method to the thermoelectric design of 2D SnSe materials and identify several novel structures with lower free energy and better thermoelectric performance than the experimental monolayer structure in theory. We hope the multi-objective Pareto Optimization method can make the integrative design of multi-objective and multi-functional materials a reality.

Waste heat is an inevitable by-product of machines that utilize energy. On the one hand, we hunt for clean, secure and sustainable new energy. On the other hand, effective utilization of existing energy sources is another avenue to boost the economic growth and social prosperity. Thermoelectric devices and materials with high efficiency are badly needed since they could directly generate electricity from waste heat, in which the efficiency is described by the dimensionless figure of merit $ZT = \sigma S^2 T / \kappa$, where interrelated S , σ and κ are the Seebeck coefficient, the electrical conductivity and the thermal conductivity, respectively. To optimize the ZT of a material, a large power factor ($S^2\sigma$) and low thermal conductivity simultaneously are required. Owing to the different extent of mean free path of electrons and phonons, each transport characteristics could be separately and elaborately tailored by band engineering [1–4], and by suppressing lattice thermal conductivity via giant phonon anharmonicity or strong phonon scattering [5–8] to maximize ZT in bulk materials.

What's more, in 2013, the White House announced the Materials Genome Initiative for Global Competitiveness (MGI)[9] aiming to, significantly, accelerate the process applying the advanced materials to the marketplace. There are some methods to guide the discovery of thermoelectric materials computationally[10]. So, with the scope of this work, we aim to search for one method to discover new stable materials, meanwhile, with the better thermoelectric performance.

Recently, bulk tin selenide (SnSe) with an extraordinary ZT of 2.6 at 923 K by Zhao *et al.* [11], shed a light over the field of thermoelectric materials. This is mostly due to its ultralow thermal conductivity ($0.3 \sim 0.4 \text{ W/mK}$). This outstanding material has rapidly aroused great attention including the theoretical exploration [12–15] and the experimental synthesis [16–18], which taps great potential in searching the novel thermoelectric materials. Even though there is a controversy about the single crystalline SnSe sample and measured thermal conductivity [19], these seminal works have made a crucial step forward to high thermoelectric performance in simple and pure bulk materials without doping or phononic crystals. At about 810 K, SnSe undergoes a second order phase transition

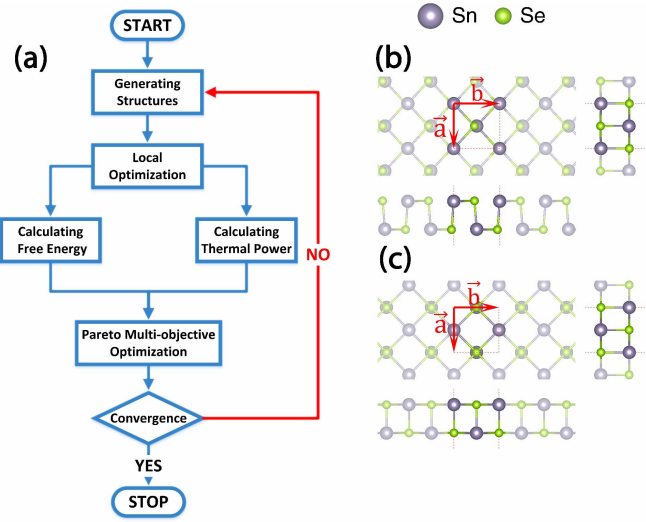


FIG. 1. (a) High-Throughput calculation scheme apdoting multi-objectives method in thermoelectric 2D SnSe. (b) Three-view drawing two typical 2D SnSe phases corresponding to the *Pnma* and *Cmcm* bulk phases. The dark gray and the green atom symbols are the Sn and Se, respectively.

from the low symmetry *Pnma* to high symmetry *CmCm* phase shown in Fig. 1(b) and (c). Because of quantum confinement effect, sometimes two dimensional (2D) materials have unexpected thermal [20], mechanical [21] and thermopower [22] compared with their pristine bulk materials. Therefore, it is interesting to explore whether the corresponding 2D SnSe may be stable and show superior thermoelectric property.

In the mapping from structure to function, microscopic atomic configuration is at the core of macroscopic properties. Thanks to the significant development of crystal structure prediction, new materials can be inversely searched by artificial intelligence such as genetic algorithm (GA) [23], particle-swarm optimization (PSO) [24] and data filtering [25] rather than the traditional costly Edisonian trial-and-error approach. Sometimes, the structures with lowest free energy do not have good thermoelectric performance and some

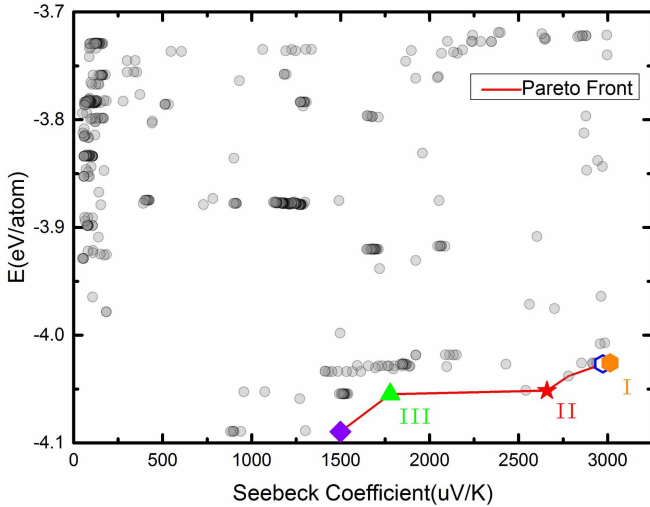


FIG. 2. The Seebeck coefficient landscape versus free energy of 2D SnSe materials at room temperature (300 K). The larger colourful symbols in the red line represent the structures in the Pareto Front with simultaneous larger thermopower and lower free energy than others with gray solid circle. The empty one in the Pareto Front corresponds to a bilayer SnSe discussed in the Supporting Information.

structures with little higher free energy (metastable) have much better in the thermoelectric properties. In this letter, we adopt an efficient and reliable method combining multi-objectives Particle Swarm Optimization (MOPSO)[26] and Non-dominated Sorting Genetic Algorithm II(NSGA-II) [27] based on the Pareto front to predict better thermoelectric 2D SnSe materials. In order to maintain accuracy and feasibility, we overlook the electrical conductivity and the lattice conductivity that are related to the controversial relaxation time [28, 29]. In the high-throughput DFT calculations, electron-phonon Wannier [30] and exactly iterative relaxation-time [31] are formidable. Hence, we simultaneously optimize free energy and Seebeck coefficient as objective functions avoiding good property but unstable structures, and bad property but stable structures. This directly targeted optimization strategy is applicable to predict new materials with superior property and stable structure at the same time. The self-consistent energy calculations and structure optimization are employed using the Perdew-Burke-Ernzerhof (PBE) exchange-correlation functional [32] along with the projector-augmented wave (PAW) potentials [33] implemented in the Vienna Ab-initio Simulation Package (VASP) [34]. Energy convergence threshold is set to 10^{-6} eV and all the atoms are allowed to relax until the maximal Hellmann-Feynman force is less than 0.001 eV/Å. The kinetic energy cut-off was 600 eV and phonon dispersion were obtained using Phonopy package [35]. The Seebeck coefficient was evaluated by BoltzTrap [36] and the MOPSO approach [37, 38] discussed here has been implemented in our homemade computer code.

The workflow for high-throughput calculation is shown in Fig. 1(a). Firstly, the initial crystal structures will be generated through atomic Wyckoff position and space groups.

Then local optimization (structure relaxation) will be done sequentially to eliminate a couple of worst structures and this crucial process will guarantee population diversity and make whole energy landscape a well-organized shape. During the structures generating process, the similar structures will be removed in order to avoid wasting calculation resources [24]. Thirdly, the Seebeck coefficient will be extracted at each temperatures. Here, as a benchmark, we only consider room temperature (300 K) data in all calculations. The next pivotal step is to apply multi-objective method to predict the lower free energy and higher Seebeck coefficient based on the Pareto Front. Different from any other single objective optimization algorithm, the leader is not one structure with unique property, such as the lowest free energy, but a leader set, named the Pareto Front including the lower free energy and the larger Seebeck coefficient than others. Generally, in a collection of structures, $\{S_n\}$, $n \in \{1, 2, \dots, N\}$, N is the number of all structures, where the $S_i, S_j \in \{S_n\}$, if the structure, S_i , possess a lower free energy and larger thermopower than another structure, S_j , which is called that S_i dominates S_j , then the S_i is regarded as Pareto Efficiency as following equations:

$$E(S_i) \leq E(S_j); \text{ and } S(S_i) \geq S(S_j).$$

where all the Pareto optimal structures constitute the Pareto Front. Then we use PSO algorithm, making the Pareto Front lead all the structures forward to the next Pareto Front with lower free energy and larger thermopower than one of the present generation. And finally, if the convergence criterion is reached, the whole procedure will stop and output the reasonable Pareto Front set. Otherwise, return and repeat all above process.

Figure 2 is the result adopting multi-objective method including 1538 samples to search the stable functional structures only based on the chemistry composition. The multi-objective method has the ability to predict novel structures with not only lower free energy, but also at the same time, higher Seebeck coefficient. The red line is the first Pareto Front set inherently having lower free energy and the larger thermopower. Interestingly, in our blind searching we have reconfirm two known 2D SnSe structures [39, 40], the violet rhombus symbol and its left nearest neighbor gray solid circle corresponding to Fig. 1(b) and (c) respectively, which validates the correctness and exhibit robustness of our computational method in high-throughput multi-objective calculation. Furthermore, three novel materials, 2D SnSe-I, 2D-SnSe-II and 2D SnSe-III, in the Pareto Front with superior stability and much larger thermopowers than the known structures.

Now let us continue to confirm the thermoelectric performance and the stability of the three novel 2D SnSe structures in the Pareto Front adopting multi-objective method, which are with little larger free energy and much larger Seebeck Coefficients than the structures in Fig. 2. The orange hexagon in Fig. 3(a) is the honeycomb monolayer, 2D SnSe-I, with small buckling on the side view similar with the silicene [41]. The blue hollow hexagon is one bilayer counterpart of the honeycomb structure. Due to the many different stacking styles,

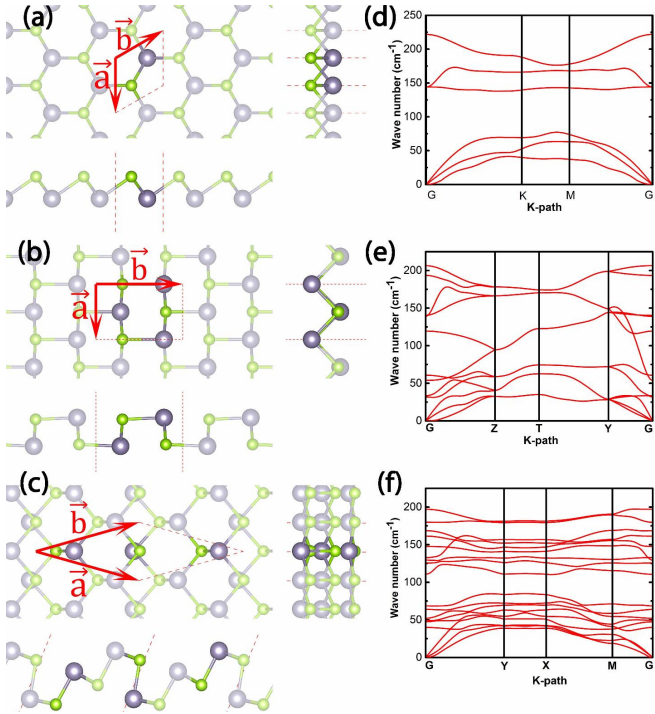


FIG. 3. Crystal three-view drawings of the novel 2D SnSe structures with superior thermal power in the Pareto Front. (a) 2D SnSe-I, (b) 2D SnSe-II and (c) 2D SnSe-III structures, respectively. (d)(e)(f) are the corresponding phonon dispersion relations.

there are a couple of gray circles around the blue one. 2D SnSe-II phase, Fig. 3(b) lie on the Pareto Font in red pentagram with armchair and zigzag ridges in the different sides. More interesting, we discover accidentally that same main group and stoichiometric number of GeSe has been synthesized by high-pressure techniques [42], which are very similar with our 2D SnSe-II material. The structure of gray solid circle, near neighbor (left one) of the red pentagram, has higher symmetry than 2D SnSe-II corresponding to the monolayer *Cmcm* phase compared with monolayer *Pnma* phase. The structure of green triangle, 2D SnSe-III, is shown in Fig. 3(c) combined with armchair and zigzag one by one viewing from one side. The optimized structural parameters, a and b , of three novel 2D SnSe are summarized in the Supporting Information.

Now our first priority is to certify the stability of these new freestanding 2D SnSe materials. The free energy of 2D SnSe-I (-3.998 eV/atom), 2D SnSe-II (-4.023 eV/atom) and 2D SnSe-III (-4.026 eV/atom) are higher than *Pnma* phase (-4.059 eV/atom). The dynamical stabilities of these metastable structures have been confirmed by phonon dispersion relations shown in Figure 3 (d), (e) and (f), respectively. For 2D materials, there are two acoustic phonon modes linear with \mathbf{q} in the vicinity of the Brillouin Zone center and the cross-plane polarized acoustic ZA mode has a quadratic dispersion near the Γ point that is a characteristic of 2D materials. Moreover, ab

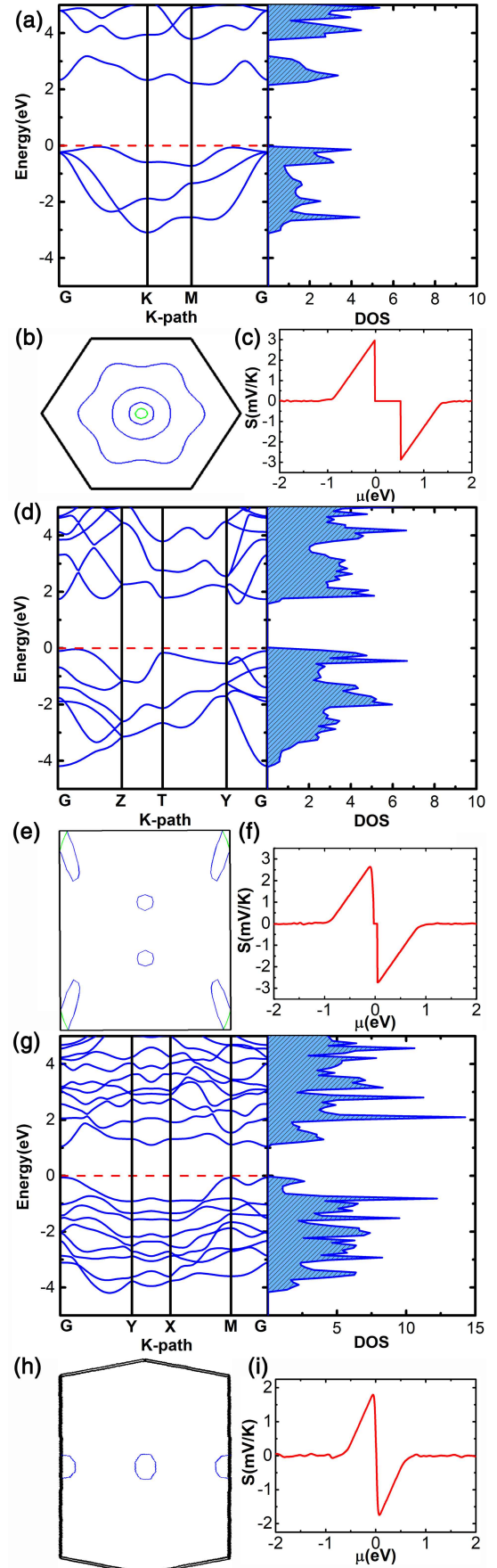


FIG. 4. (a) (d) (g) Electronic band structures, total density of states,(b) (e) (h) Fermi surface below 100meV top of valence band and (c) (f) (i) Seebeck coefficient of the 2D SnSe-I, 2D SnSe-II and 2D SnSe-III structures, respectively. The fermi energy is setted as 0ev which is the dotted line in the corresponding electronic band structure.

initio molecular dynamics (AIMD) simulations using canonical ensemble at a series of elevated temperatures with lifetime longer than 10 ps was performed to verify their stability shown in the Supporting Information. Phonon dispersion relations indicate that the thermal conductivities of SnSe-II and SnSe-III are lower than the SnSe-I phase.

Electronic band structures, density of states, band degeneracy and Seebeck coefficient of 2D SnSe-I, 2D SnSe-II and 2D SnSe-III, are shown in Fig. 4. We can see that in the structure 2D SnSe-I, the valance band maximum (VBM) is in the G-K path, and the conduction band minimum (CBM) is in the M-G path in the Brillouin Zone (BZ) with indirect band gap of 2.21 eV around the Fermi level. For the 2D SnSe-II, the VBM is in the Y-G path, the CBM is in the G-Z path with the indirect band gap of 1.62 eV smaller than the 2D SnSe-I. Furthermore, in the 2D SnSe-III, both VBM and CBM are in the G point with direct band gap of 1.11 eV that is least bandgap among these three structures. Their band gaps are larger than that of the monolayer *Pnma* phase (0.941 eV[12]).

Fig. 4 (c), (f) and (i) are the Seebeck coefficient dependent of the chemical potential μ corresponding to the 2D SnSe-I, 2D SnSe-II, 2D SnSe-III structures respectively. The sign of Seebeck illustrate that dominate carrier transport. Positive or negative S correspond to the hole carrier (p-type and $\mu < 0$) or eletron carrier (n-type and $\mu > 0$). The maximum of Seebeck coefficient of SnSe-I, SnSe-II and SnSe-III are 2964 ($\mu\text{V}/\text{K}$) 2726 ($\mu\text{V}/\text{K}$) and 1795 ($\mu\text{V}/\text{K}$) which are much larger than the known 2D SnSe monolayer of *Pnma* phase (around 1600 ($\mu\text{V}/\text{K}$)) [28] and 3-5 times of bulk SnSe (500-580 ($\mu\text{V}/\text{K}$)) [46] at PBE level.

Mahan-Sofo theory [47] estimates Seebeck coefficient using effective mass can be expressed as following equation:

$$S = \frac{8\pi^2 k_B^2 T}{3q h^2} m_d^* \left(\frac{\pi}{3n}\right)^{2/3}, \quad (1)$$

where h is Planck constant. Because Seebeck is proportional to the density of states (DOS) effective mass m_d^* . Therefore, the narrower the electronic band, the larger the effective mass that lead to larger Seebeck coefficients [2]. For 2D materials, the relation between density of states effective mass and band effective mass is

$$m_d^* = N_b * m_b^*, \quad (2)$$

where the m_d^* is DOS effective mass, the N_b is the band degeneracy, and the m_b^* is the band effective mass. The band degeneracy of the electronic band structure plays a very important role in the band engineering about improving the thermoelectric performance. In the context of p-semiconductor, the fermi energy is close to the top of valence band, so for the three 2D structures, the fermi surfaces within 100meV from the top of valence band in the first Brillouin zone are calculated shown in the Fig. 4 (b), (e) and (h), and the high-symmetry points are given. The band degeneracy, N_b , is 4, 4, 2 corresponding to the 2D SnSe-I, 2D SnSe-II, 2D SnSe-III structures respectively.

On the one hand, we use multi-objective method thus higher Seebeck coefficient is one of the intrinsic optimization objective besides the lower free energy. One the other hand, based on the Mott formula [47],

$$S = \frac{\pi^2 k_B^2 T}{3q} \cdot \left\{ \frac{d[\ln(\sigma(E))]}{dE} \right\}_{E=E_F}. \quad (3)$$

If the specific system or materials has a local substantially increase of the density of states over a small energy scale E, the Seebeck will be enhanced. In the expression, energy-dependent electrical conductivity $\sigma(E) = g(E)f(E)q\mu$, in which $f(E)$, $g(E)$, q , k_B , and μ are the Fermi-Dirac distribution function, the density of states, carrier charge, Boltzmann constant and the mobility. Furthermore, strong asymmetry of the density of states is another reason leading to our large Seebeck compared with previous structures.

Generally, there are three mainstream approach to enhance Seebeck coefficient. High valley degeneracy produced by carrier pocket enginerring [1], a distorted density of states by doping that resonates one energy level of a localized atom [2], weak electron-phonon coupling [43], phonon drag effect [44] and puddling-mold-like shape in the highest valence band or lowest conduction band that is beneficial to a high Seebeck and conductivity [45]. Around the Fermi level, as local increment in the DOS becomes sharper and the effective mass become larger, the Seebeck coefficient will be larger.

In conclusion, we have applied the multi-objective Pareto Optimization method based on the Pareto Efficiency and Pareicle-Swarm Optimization to directionally design functional materials only according to the chemistry composition. This method has the ability to design the structures with having not only lower free energy but also larger Seebeck coefficient, at one time. Further more, the Pareto Optimization shows the great potential to design more wide kinds of stable and multi-functional materials, where multiple material properties are in demands instead of the thermoelectric property. The designed substantial novel structures in the Pareto Front also indicates that the group IV-VI and group-V may share similar homogeneous configurations with the similar outer valence electrons. Specially, there are abundant 2D structures which are similar with the discovered 2D Phosphorus sheets [42, 48–50]. Hence, the efficiency of Pareto Optimization of structures has demonstrated that it is instructive to the further materials design and maybe even the experimental synthesis.

This work is supported by the NSFC with grant No. 11775159, the National Youth 1000 Talents Program in China, and the startup Grant at Tongji University.

* S. Yan and Z. Gao contributed equally to this work

† Corresponding Email: Xonics@tongji.edu.cn

- [1] Y. Pei, X. Shi, A. LaLonde, H. Wang, L. Chen, and G. J. Snyder, *Nature* **473**, 66 (2011).
- [2] J. P. Heremans, V. Jovovic, E. S. Toberer, A. Saramat,

- K. Kurosaki, A. Charoenphakdee, S. Yamanaka, and G. J. Snyder, *Science* **321**, 554 (2008).
- [3] W. Zhao, P. Wei, Q. Zhang, H. Peng, W. Zhu, D. Tang, J. Yu, H. Zhou, Z. Liu, X. Mu, *et al.*, *Nature communications* **6** (2015).
- [4] M. S. Dresselhaus, G. Chen, M. Y. Tang, R. Yang, H. Lee, D. Wang, Z. Ren, J.-P. Fleurial, and P. Gogna, *Advanced Materials* **19**, 1043 (2007).
- [5] O. Delaire, J. Ma, K. Marty, A. F. May, M. A. McGuire, M.-H. Du, D. J. Singh, A. Podlesnyak, G. Ehlers, M. Lumsden, *et al.*, *Nature materials* **10**, 614 (2011).
- [6] D. Morelli, V. Jovovic, and J. Heremans, *Physical review letters* **101**, 035901 (2008).
- [7] C. W. Li, J. Hong, A. F. May, D. Bansal, S. Chi, T. Hong, G. Ehlers, and O. Delaire, *Nature Physics* (2015).
- [8] W. Kim, J. Zide, A. Gossard, D. Klenov, S. Stemmer, A. Shakouri, and A. Majumdar, *Physical Review Letters* **96**, 045901 (2006).
- [9] J. P. Holdren *et al.*, National Science and Technology Council OSTP. Washington, USA (2011).
- [10] P. Gorai, V. Stevanovi, and E. S. Toberer, **2**, natrevmats201753 (2017).
- [11] L.-D. Zhao, S.-H. Lo, Y. Zhang, H. Sun, G. Tan, C. Uher, C. Wolverton, V. P. Dravid, and M. G. Kanatzidis, *Nature* **508**, 373 (2014).
- [12] F. Q. Wang, S. Zhang, J. Yu, and Q. Wang, *Nanoscale* **7**, 15962 (2015).
- [13] D. Bansal, J. Hong, C. W. Li, A. F. May, W. Porter, M. Y. Hu, D. L. Abernathy, and O. Delaire, *Physical Review B* **94**, 054307 (2016).
- [14] M. Mehboudi, B. M. Fregoso, Y. Yang, W. Zhu, A. van der Zande, J. Ferrer, L. Bellaiche, P. Kumar, and S. Barraza-Lopez, *Physical review letters* **117**, 246802 (2016).
- [15] J. M. Skelton, L. A. Burton, S. C. Parker, A. Walsh, C.-E. Kim, A. Soon, J. Buckeridge, A. A. Sokol, C. R. A. Catlow, A. Togo, *et al.*, *Physical review letters* **117**, 075502 (2016).
- [16] L. Li, Z. Chen, Y. Hu, X. Wang, T. Zhang, W. Chen, and Q. Wang, *Journal of the American Chemical Society* **135**, 1213 (2013).
- [17] C. Zhang, H. Yin, M. Han, Z. Dai, H. Pang, Y. Zheng, Y.-Q. Lan, J. Bao, and J. Zhu, *ACS nano* **8**, 3761 (2014).
- [18] S. Zhao, H. Wang, Y. Zhou, L. Liao, Y. Jiang, X. Yang, G. Chen, M. Lin, Y. Wang, H. Peng, *et al.*, *Nano Research* **8**, 288 (2015).
- [19] P.-C. Wei, S. Bhattacharya, J. He, S. Neeleshwar, R. Podila, Y. Chen, and A. Rao, *Nature* **539**, E1 (2016).
- [20] X. Xu, L. F. Pereira, Y. Wang, J. Wu, K. Zhang, X. Zhao, S. Bae, C. T. Bui, R. Xie, J. T. Thong, *et al.*, *Nature communications* **5** (2014).
- [21] Z. Gao, X. Dong, N. Li, and J. Ren, *Nano letters* **17**, 772 (2017).
- [22] S. Shimizu, M. S. Bahramy, T. Iizuka, S. Ono, K. Miwa, Y. Tokura, and Y. Iwasa, *Proceedings of the National Academy of Sciences* **113**, 6438 (2016).
- [23] A. R. Oganov and C. W. Glass, *The Journal of chemical physics* **124**, 244704 (2006).
- [24] Y. Wang, J. Lv, L. Zhu, and Y. Ma, *Physical Review B* **82**, 094116 (2010).
- [25] S. Lebègue, T. Björkman, M. Klintenberg, R. M. Nieminen, and O. Eriksson, *Physical Review X* **3**, 031002 (2013).
- [26] S. Mostaghim and J. Teich, in *Swarm Intelligence Symposium, 2003. SIS'03. Proceedings of the 2003 IEEE* (IEEE, 2003) pp. 26–33.
- [27] K. Deb, A. Pratap, S. Agarwal, and T. Meyarivan, *IEEE transactions on evolutionary computation* **6**, 182 (2002).
- [28] D. I. Bilc, G. Hautier, D. Waroquiers, G.-M. Rignanese, and P. Ghosez, *Physical review letters* **114**, 136601 (2015).
- [29] A. Cepellotti and N. Marzari, *Physical Review X* **6**, 041013 (2016).
- [30] F. Giustino, M. L. Cohen, and S. G. Louie, *Physical Review B* **76**, 165108 (2007).
- [31] W. Li, J. Carrete, N. A. Katcho, and N. Mingo, *Computer Physics Communications* **185**, 1747 (2014).
- [32] J. P. Perdew, K. Burke, and M. Ernzerhof, *Physical review letters* **77**, 3865 (1996).
- [33] P. E. Blöchl, *Physical review B* **50**, 17953 (1994).
- [34] G. Kresse and J. Furthmüller, *Physical review B* **54**, 11169 (1996).
- [35] A. Togo, F. Oba, and I. Tanaka, *Physical Review B* **78**, 134106 (2008).
- [36] G. K. Madsen and D. J. Singh, *Computer Physics Communications* **175**, 67 (2006).
- [37] M. Núñez-Valdez, Z. Allahyari, and A. R. Oganov, *arXiv preprint arXiv:1610.07824* (2016).
- [38] Y.-Y. Zhang, W. Gao, S. Chen, H. Xiang, and X.-G. Gong, *Computational Materials Science* **98**, 51 (2015).
- [39] F. Q. Wang, S. Zhang, J. Yu, and Q. Wang, *Nanoscale* **7**, 15962 (2015).
- [40] L.-C. Zhang, G. Qin, W.-Z. Fang, H.-J. Cui, Q.-R. Zheng, Q.-B. Yan, and G. Su, *Scientific reports* **6** (2016).
- [41] S. Cahangirov, M. Topsakal, E. Aktürk, H. Şahin, and S. Ciraci, *Physical review letters* **102**, 236804 (2009).
- [42] F. O. von Rohr, H. Ji, F. A. Cevallos, T. Gao, N. P. Ong, and R. J. Cava, *Journal of the American Chemical Society* **139**, 2771 (2017).
- [43] H. Wang, Y. Pei, A. D. LaLonde, and G. J. Snyder, *Proceedings of the National Academy of Sciences* **109**, 9705 (2012).
- [44] H. Ohta, S. Kim, Y. Mune, T. Mizoguchi, K. Nomura, S. Ohta, T. Nomura, Y. Nakanishi, Y. Ikuhara, M. Hirano, *et al.*, *Nature materials* **6**, 129 (2007).
- [45] K. Kuroki and R. Arita, *Journal of the Physical Society of Japan* **76**, 083707 (2007).
- [46] A. Dewandre, O. Hellman, S. Bhattacharya, A. H. Romero, G. K. Madsen, and M. J. Verstraete, *Physical review letters* **117**, 276601 (2016).
- [47] G. Mahan and J. Sofo, *Proceedings of the National Academy of Sciences* **93**, 7436 (1996).
- [48] J. Guan, Z. Zhu, and D. Tománek, *Physical review letters* **113**, 046804 (2014).
- [49] W. H. Han, S. Kim, I. H. Lee, and K. J. Chang, *Journal of Physical Chemistry Letters* , 4627 (2017).
- [50] L. Li, J. Kim, C. Jin, G. J. Ye, D. Y. Qiu, H. Felipe, Z. Shi, L. Chen, Z. Zhang, F. Yang, *et al.*, *Nature nanotechnology* **12**, 21 (2017).